Quantum dynamics of Raman-coupled Bose-Einstein condensates using Laguerre-Gaussian beams

Rina Kanamoto, Ewan M. Wright, and Pierre Meystre
Department of Physics and College of Optical Sciences, The University of Arizona, Tucson, Arizona 85721, USA
(Received 27 February 2007; published 21 June 2007)

We investigate the quantum dynamics of Raman-coupled Bose-Einstein condensates driven by laser beams that carry orbital angular momentum. By adiabatically eliminating the excited atomic state we obtain an effective two-state Hamiltonian for the coupled condensates, and quantization of the matter-wave fields results in collapse and revivals in the quantum dynamics. We show that the revival period depends on whether the initial nonrotating condensate displays broken U(1) symmetry or not, and that the difference may be detected by measuring the motion of quantized vortices that are nested in the density profile of the Raman-coupled condensates. We further study the steady-state population transfer using a linear sweep of the two-photon detuning, by which the atomic population is coherently transferred from an initial nonrotating state to the final vortex state.

DOI: 10.1103/PhysRevA.75.063623 PACS number(s): 03.75.Kk, 03.75.Lm, 03.75.Mn

I. INTRODUCTION

Controlling and probing of the quantum state of cold atoms or molecules are opening up new frontiers for exploring the fundamentals of quantum mechanics. At the ultracold temperatures characteristic of Bose-Einstein condensates (BECs) matter reveals its wave character, and the quantum statistics of the atoms or molecules play an important role. By controlling both the atomic collisions and the properties of laser fields applied to a BEC, one may generate tailor made quantum states of matter. For example, photons and atoms can interchange mechanical momentum, and atoms can therefore be prepared into a specific center-of-mass momentum state by the appropriate choice of spatial light field profile [1,2]. The light field may also be used for the detection of the atomic quantum state [3].

A commonly applied notion for atomic BECs is that of Bose broken symmetry (BBS) [4–7], or broken U(1) symmetry, whereby the state vector for the BEC is described via a wave packet of states of varying atom number N. In this scheme the fact that the atom number is not fixed is traded off for the fact that the macroscopic wave function for the BEC, obtained as the expectation value of the field annihilation operator, acquires a definite phase, hence the name broken U(1) symmetry. The BBS approach is typified by the use of a coherent-state description for the state of a BEC. In contrast, a number conserving (NC) approach is also possible, but in that case the phase of the corresponding macroscopic wave function has no physical significance, and U(1) symmetry is preserved. In the absence of atomic collisions, it is known that whether or not the U(1) symmetry is broken does not affect any physical observables, and whether one describes the state of the BEC as a coherent state or a number state is largely a matter of calculational convenience [5,7]. Furthermore, for the case involving the interference between two BECs, even for an initial state with a fixed number of atoms, quantum coherence is built up by the measurement process which leads to uncertainty in the atom number, and the resulting interference pattern is indistinguishable from that which would have resulted from a coherent state description [8,9].

However, this equivalence between the BBS and NC approaches holds only when atomic collisions can be neglected. If one takes atomic collisions into account differences between the two approaches appear in the collapse and revival times that can occur in the interference between BECs with different spatial modes, for example in the interference between condensates [10,11], a double-well system [12], or in Ramsey fringe-type experiments [13]. Intuitively, the revival period difference arises from the fact that the allowed number difference ΔN between the two BECs is different for the two cases: In the NC approach ΔN is always an even integer, whereas in the coherent state approach based on BBS ΔN can be an arbitrary integer. Since atomic collisions lead to matter wave phase shifts proportional to the atom number, the interference between two BECs, which depends on ΔN, is markedly different depending on whether U(1) symmetry is broken or not, and leads to a factor of two difference in the revival period between the two approaches. This factor of two difference has recently been observed for the first time in an experiment that looks at the interference between atoms released from a lattice of double well systems [14]: Depending on the preparation conditions, the atoms trapped in each individual double well in the lattice may be best described as a number state or a coherent state, and this leads to a factor of two difference in the revival time in the interference pattern that arises when the atoms are released and allowed to interfere.

Collapse and revivals have previously been investigated experimentally in the Jaynes-Cummings model of a two-level atom interacting with a quantized laser field [15], wave packet dynamics of Rydberg atoms [16], matter waves in an optical lattice [17], and most recently for a matter wave in a lattice of double wells [14]. Nevertheless, the use of collapse and revivals to test the fundamental notion of U(1) broken-symmetry as applied to a *single* BEC via the period of the collapse and revivals has not been realized experimentally so far. Walls and co-workers [10,11] showed that this could be realized by coupling an initial BEC with a given mode structure to a second BEC mode, thereby realizing a two-mode system. The period of the revivals of the system would then

act as a test of whether or not the initial isolated BEC exhibited BBS or not. Search [13] has proposed precisely such an experiment based on a Ramsey fringe approach, but this has not been realized to date.

In this paper, we consider the case of Raman-coupled BECs using Laguerre-Gaussian (LG) beams [18] as a potential testing ground for the BBS description of an initial BEC. Because of the helical phase structure of the laser fields, orbital angular momentum (OAM) is transferred from the light to the atoms and results in a BEC in a coherent superposition of two components with distinct center-of-mass OAM [18–20]. (In another scheme for generating vortices a decentered Gaussian beam is rotated around the center of a trapped BEC [21], but we do not analyze that case here.) By considering BECs with relatively small numbers of atoms, and quantizing the matter-wave fields, the system can be mapped onto a Hamiltonian that describes the dynamics of an ideal two-mode system. Then the granular nature of the matter-wave field becomes important, and we explore the collapse and revivals in the system both with and without broken U(1) symmetry. In particular, we show that the difference between the two approaches is directly visible in the motion of quantized vortices that appear in the density profile of the Raman-coupled condensates, the density profile being a relatively easy physical quantity to observe. To put our proposal in context, collapse and revival dynamics have previously been observed using the spatial density profile in a two-component ^{87}Rb BEC [22], and the Raman vortex coupler using LG beams has now been realized experimentally [23], both of these experiments being performed for large atom numbers where the granular nature of the matter wave fields is not relevant.

This paper is organized as follows. In Sec. II we formulate the problem, and map the three-level Λ-type atomic system coupled with LG fields onto a two-mode Hamiltonian in the angular-momentum representation. In Sec. III, we focus on the collapse and revival dynamics for initial number states and coherent states for the BEC, and show that these may be measured using the spatial density profile of the Raman-coupled condensates as well as the atom statistics. Section IV summarizes the results in this paper, mentioning the time-dependent two-photon detuning for the stimulated Raman population transfer.

II. FORMULATION OF THE PROBLEM

In this section we formulate the two-mode approximation for two Raman-coupled BECs and introduce the angular momentum representation used to solve the quantum dynamical system.

A. Hamiltonian

We consider a quantum-degenerate sample of ultracold bosonic atoms with three participating levels $|a\rangle$, $|b\rangle$, and $|e\rangle$ arranged in a Λ configuration, see Fig. 1. The sample is irradiated by a pair of laser fields of frequencies $\omega_{1,2}$, transitions between $|a\rangle$ and $|b\rangle$ being dipole forbidden. The system Hamiltonian $\hat{H}=\hat{H}_A+\hat{H}_{\mathrm{AF}}$ is given by [24]

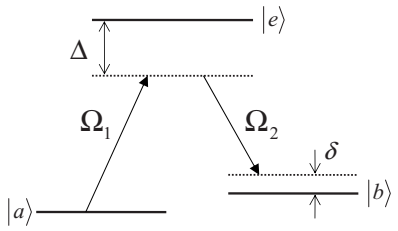

FIG. 1. Λ atomic level scheme: Three hyperfine states $|a\rangle$, $|b\rangle$, and $|e\rangle$ are coupled with light fields of Rabi frequencies Ω_1,Ω_2, and laser frequencies ω_1, ω_2, respectively. The common detuning Δ is sufficiently large that the excited state $|e\rangle$ is not significantly populated.

$$\hat{H}_A = \sum_{j=a,b,e} \int d^3r\, \hat{\Psi}_j^\dagger(\boldsymbol{r})\hat{H}_0^{(j)}\hat{\Psi}_j(\boldsymbol{r}) + \frac{1}{2}\sum_{j,j'=a,b,e}\chi_{jj'}\int d^3\, r\hat{\Psi}_j^\dagger(\boldsymbol{r})\hat{\Psi}_{j'}^\dagger(\boldsymbol{r})\hat{\Psi}_{j'}(\boldsymbol{r})\hat{\Psi}_j(\boldsymbol{r}), \quad (1)$$

$$\hat{H}_{\mathrm{AF}} = -\hbar\int d^3r[\hat{\Psi}_e^\dagger(\boldsymbol{r})\hat{\Psi}_a(\boldsymbol{r})\Omega_1^{(+)}(\boldsymbol{r})e^{-i\omega_1 t} + \mathrm{H.c.} + \hat{\Psi}_e^\dagger(\boldsymbol{r})\hat{\Psi}_b(\boldsymbol{r})\Omega_2^{(+)}(\boldsymbol{r})e^{-i\omega_2 t} + \mathrm{H.c.}], \quad (2)$$

where $\hat{\Psi}_j^\dagger, \hat{\Psi}_j$ are creation and annihilation field operators for bosonic atoms in the states $j=a,b,e$. Atomic collisions are included via the pseudopotential coefficients $\chi_{jj'}=4\pi\hbar^2 a_{jj'}/M$, where $a_{jj'}$ is the s-wave scattering length between two atoms in the states j and j', and M is the atomic mass. The coupling of the atoms to the classical optical fields is described by the Rabi frequencies $\Omega_{1,2}^{(\pm)}$, where $\pm$ denotes the positive and negative frequency components. The atoms are further supposed to be confined in harmonic traps, so that the center-of-mass Hamiltonian for atoms in each state $j=a,b,e$ is given by

$$\hat{H}_0^{(j)} = -\frac{\hbar^2\nabla^2}{2M} + V_j(\boldsymbol{r}), \quad (3)$$

$$V_j(\boldsymbol{r}) = \frac{M\omega_{r,j}^2(x^2+y^2)}{2} + \frac{M\omega_{z,j}^2 z^2}{2}, \quad (4)$$

with $\omega_{r,j}$ and $\omega_{z,j}$ the oscillator frequencies along the radial (r) and longitudinal (z) directions for the different atomic states.

If the detuning Δ from the excited state $|e\rangle$ is sufficiently large (see Fig. 1), the population of that state remains negligible and spontaneous emission may be neglected. The excited state can then be adiabatically eliminated as

$$\hat{\Psi}_e(\boldsymbol{r}) = \frac{1}{\Delta}[\Omega_1^{(+)}(\boldsymbol{r})\hat{\Psi}_a(\boldsymbol{r})e^{-i\omega_1 t} + \Omega_2^{(+)}(\boldsymbol{r})\hat{\Psi}_b(\boldsymbol{r})e^{-i\omega_2 t}] \quad (5)$$

and the Hamiltonian for the atom-field interaction reduces to

$$\hat{H}_{\mathrm{AF}} = \frac{-2\hbar}{\Delta} \int d^3r [\Omega_1^{(+)} \Omega_2^{(-)} e^{i(\omega_2-\omega_1)t} \hat{\Psi}_b^\dagger \hat{\Psi}_a + \mathrm{H.c.}], \quad (6)$$

where we have omitted the diagonal terms due to the ac-stark shift, which create an effective potential for the atoms but do not affect the dynamics. The atom-field interaction Hamiltonian H_{AF} in Eq. (6) reflects the fact that if an atom makes a transition from state $|a\rangle$ to the excited state via absorption of a photon of frequency ω_1, this will be rapidly followed by emission of a photon of frequency ω_2 and a Raman transition to the state $|b\rangle$.

Bringing these results together, the system Hamiltonian $\hat{H}=\hat{H}_A+\hat{H}_{\mathrm{AF}}$ is now given by

$$\hat{H}_A = \sum_{j=a,b} \int d^3r\, \hat{\Psi}_j^\dagger \hat{H}_0^{(j)} \hat{\Psi}_j + \sum_{j,j'=a,b} \frac{\chi_{jj'}}{2} \int d^3r\, \hat{\Psi}_j^\dagger \hat{\Psi}_{j'}^\dagger \hat{\Psi}_{j'} \hat{\Psi}_j,$$

$$\hat{H}_{\mathrm{AF}} = \frac{-2\hbar}{\Delta} \int d^3r [\Omega_1^{(+)} \Omega_2^{(-)} e^{i(\omega_2-\omega_1)t} \hat{\Psi}_b^\dagger \hat{\Psi}_a + \mathrm{H.c.}]. \quad (7)$$

This Hamiltonian is the starting point for our analysis.

B. Orbital angular momentum of light

Light has two kinds of angular momentum: A spin-angular momentum associated with its polarization, and an orbital angular momentum (OAM) associated with mechanical rotation [25]. The system described by the Hamiltonian (7) corresponds to a familiar coherent coupler between the atomic BECs in the states $|a\rangle$ and $|b\rangle$ if both light fields are plane waves or Gaussian beams, that is, beams that carry no OAM. Then the absorption-emission process transfers the atom from the state $|a\rangle$ to the state $|b\rangle$ that is shifted in momentum by the two-photon recoil. On the other hand, if one or both of those laser fields carries OAM, the light field can impart its OAM to the atoms, and hence angular-momentum transfer occurs associated with the coherent coupling [26]. In this case, the two-photon recoil is associated with the difference of angular momenta of two light beams, and one realizes a Raman vortex coupler. The Raman vortex coupler has previously been studied theoretically in the limit of large atom numbers where a treatment based on coupled Gross-Pitaevskii equations is applicable [18], and an experimental realization of this case has been reported [23]. Here we explore the opposite limit of low atom numbers, where the granular nature of the quantum matter wave fields becomes relevant.

A typical set of light fields that carry OAM are Laguerre-Gaussian beams whose mode functions at the beam waist $z=0$ are given by [25]

$$\mathcal{LG}_p^l(r,\varphi) \propto (-1)^p \left(\frac{r}{w_0}\right)^{|l|} L_p^{|l|}\left(\frac{r^2}{w_0^2}\right) e^{-r^2/2w_0^2} e^{il\varphi}, \quad (8)$$

where w_0 is the focused spot size at $z=0$, p is the radial mode number, l the winding number, which describes the helical structure of the wave front, and

$$L_p^{|l|}(r) = \sum_{j=0}^{p} \frac{(|l|+p)!(-r)^j}{(p-j)!(|l|+j)!j!}, \quad (9)$$

are Laguerre polynomials. By using LG modes for the Raman coupling between the matter wave fields in the Hamiltonian (7) we can therefore create a matter-wave vortex even though the initial state is nonrotating. Henceforth, we consider only the LG modes with $p=0$, and we thus need only consider one quantum number l, to specify the OAM.

C. Two-mode Hamiltonian

We assume that all atoms are initially in the state $|a\rangle$ with total angular momentum zero, and that this state is Raman-coupled to the state $|b\rangle$ with a winding number l by using a pair of LG laser fields, one with a winding number zero and the other with winding number l. We further assume that two-body interactions are weak enough, and the external harmonic trapping frequencies $\omega_{r,j}=\omega_r$ and $\omega_{z,j}=\omega_z$ are large enough, that the mode profiles of the two atomic states are not significantly modified from their single particle forms $\psi_{0,l}(\boldsymbol{r})$ [12,27].

Under these assumptions the matter-wave field operator may be expressed as

$$\hat{\Psi}(\boldsymbol{r},t) = \hat{a}(t)\psi_0(\boldsymbol{r}) + \hat{b}(t)\psi_l(\boldsymbol{r}), \quad (10)$$

where $\hat{a}$ and $\hat{b}$ are the bosonic annihilation operators for the states $|a\rangle$ and $|b\rangle$, and the positive frequency components of the Rabi frequencies are

$$\Omega_1^{(+)}(\boldsymbol{r}) = \Omega_1 \phi_l(\boldsymbol{r}), \quad \Omega_2^{(+)}(\boldsymbol{r}) = \Omega_2 \phi_0(\boldsymbol{r}). \quad (11)$$

When the LG beam remains well collimated over the longitudinal extent of the condensate, $d_z \ll k_0 w^2/2$, the laser mode functions $\phi_{0,l}$ at the beam waist and the condensate mode functions $\psi_{0,l}$ may be expressed as

$$\phi_l(\boldsymbol{r}) = \frac{1}{\sqrt{l!\,\pi}} \left(\frac{r}{w_0}\right)^l e^{-r^2/2w_0^2} e^{il\varphi} e^{ikz}, \quad (12)$$

$$\psi_l(\boldsymbol{r}) = \frac{1}{\sqrt{l!\,\pi d_r^2}} \left(\frac{r}{d_r}\right)^l e^{-r^2/2d_r^2} e^{il\varphi} \psi_z(z). \quad (13)$$

We assume that $l>0$, and that the radial and longitudinal atomic oscillator ground state widths are the same for both atomic states $d_r=\sqrt{\hbar/(M\omega_r)}$, and $d_z=\sqrt{\hbar/(M\omega_z)}$ [28]. We further assume that the longitudinal trapping is much stronger than the radial trapping, $d_r>d_z$, and that the longitudinal wave function remains fixed as the ground state $\psi_z(z) = e^{-z^2/2d_z^2}/\sqrt{\pi^{1/2} d_z}$. The two-mode approximation is then valid under the conditions $Na_{ij} \lesssim d_k$ [12], where $i,j=a,b$ and $k=r,z$.

Substituting Eqs. (10)–(12) into the system Hamiltonian (7) with $E_j=\int d^3r\, \psi_j^* \hat{H}_0 \psi_j$, and transforming to a rotating frame using the unitary transformation $U_0 = \exp\{-i[E_a(\hat{a}^\dagger\hat{a}+\hat{b}^\dagger\hat{b})/\hbar - (\omega_2-\omega_1)\hat{b}^\dagger\hat{b}]t\}$, finally yields the reduced two-mode Hamiltonian

$$\hat{H} = \hbar\omega_r[(l + \delta/\omega_r)\hat{b}^\dagger\hat{b} + G_{aa}\hat{a}^\dagger\hat{a}^\dagger\hat{a}\hat{a} + G_{bb}\hat{b}^\dagger\hat{b}^\dagger\hat{b}\hat{b} + 2G_{ab}\hat{a}^\dagger\hat{b}^\dagger\hat{b}\hat{a} - g(\hat{a}^\dagger\hat{b} + \hat{a}\hat{b}^\dagger)], \quad (14)$$

where we have defined $\delta=\omega_2-\omega_1+(E_b-E_a)/\hbar$ as the two-photon detuning, which may be controlled experimentally. The dimensionless coupling constants for the atom-atom and atom-light interactions are given by

$$G_{jj'} = \frac{\chi_{jj'}V_{jj'j'j}}{2\hbar\omega_r} \quad (j,j' = a,b), \quad (15)$$

$$g = \frac{2\Omega_1\Omega_2 U_{0ll0}}{\omega_r\Delta}, \quad (16)$$

with

$$V_{klmn} = \int d^3r\, \psi_k^*\psi_l^*\psi_m\psi_n = \frac{1}{2\pi d_r^2\sqrt{2\pi d_z^2}}\frac{(k+l)!\,\delta_{k+l=m+n}}{2^{k+l}\sqrt{k!l!m!(k+l-m)!}}, \quad (17)$$

$$U_{klmn} = \int d^3r\, \psi_k^*\phi_l^*\psi_m\phi_n = \frac{\zeta^{k+2l-m}}{\pi(\zeta^2+1)^{k+l+1}}\frac{(k+l)!\,\delta_{k+l=m+n}}{\sqrt{k!l!m!(k+l-m)!}}. \quad (18)$$

The parameter $\zeta \equiv d_r/w_0$ characterizes the ratio of the radial oscillator ground state width to the focused light spot size, and the Kronecker delta enforces angular-momentum conservation for the atom-field interactions. Henceforth the energies, lengths, and angular momenta are measured in units of $\hbar\omega_r$, d_r, and $\hbar$, respectively.

D. Angular-momentum representation

In order to study the quantum dynamics described by the Hamiltonian (14), we introduce the following operator combinations that map our problem to Schwinger's angular-momentum representation [12],

$$\hat{J}_+ = \hat{a}\hat{b}^\dagger, \quad \hat{J}_- = \hat{a}^\dagger\hat{b}, \quad (19)$$

$$\hat{J}_x = \frac{1}{2}(\hat{J}_+ + \hat{J}_-), \quad (20)$$

$$\hat{J}_y = \frac{1}{2i}(\hat{J}_+ - \hat{J}_-), \quad (21)$$

$$\hat{J}_z = \frac{1}{2}(\hat{b}^\dagger\hat{b} - \hat{a}^\dagger\hat{a}). \quad (22)$$

These operators obey the SU(2) commutation relations $[\hat{J}_i,\hat{J}_j]=i\epsilon_{ijk}\hat{J}_k$ where ϵ_{ijk} denotes the Levi-Civita antisymmetric symbol, and the Casimir invariant is found to be $\hat{J}^2=\hat{J}_x^2+\hat{J}_y^2+\hat{J}_z^2=j(j+1)$ with $j=N/2$. For the basis $|j,m\rangle$ with $m=-j,-j+1,\ldots,j$, which are eigenstates of $\hat{J}_z$, the operators satisfy

$$\hat{J}_z|j,m\rangle = m|j,m\rangle, \quad (23)$$

$$\hat{J}^2|j,m\rangle = j(j+1)|j,m\rangle, \quad (24)$$

$$\hat{J}_\pm|j,m\rangle = \sqrt{(j\pm m+1)(j\mp m)}|j,m\rangle. \quad (25)$$

In the angular-momentum representation the Hamiltonian (14) then becomes

$$\hat{H} = h_z\hat{J}_z + \chi\hat{J}_z^2 - 2g\hat{J}_x, \quad (26)$$

where

$$h_z = l + \delta - (N-1)\chi_-, \quad (27)$$

$$\chi_- = G_{aa} - G_{bb}, \quad \chi = G_{aa} + G_{bb} - 2G_{ab}. \quad (28)$$

The angular basis states $|j,m\rangle$ and the Fock basis states $|n_a,n_b\rangle_F$ are related by $|j,m\rangle=|N/2-m,N/2+m\rangle_F$.

III. QUANTUM DYNAMICS

In this section we explore the quantum dynamics of the two-mode model, first with no atomic collisions, and then we study the collapse and revivals that occur with atomic collisions. In particular, we highlight that the collapse and revivals may be monitored by following the motion of quantized vortices that appear in the spatial density profile, and we shall also study the resulting atom statistics.

A. No atomic collisions

In the absence of atomic collisions, $G_{ij}=0$, giving $h_z=l+\delta$ and $\chi=0$, the two-mode Hamiltonian reduces to the form of two simple coupled harmonic oscillators. Then the solution of the Heisenberg equations of motions for $\hat{a}(t)$ and $\hat{b}(t)$ is found to be

$$\begin{bmatrix}\hat{a}(t)\\ \hat{b}(t)\end{bmatrix} = e^{-i(l+\delta)/2}\begin{bmatrix}\mathcal{A}(t) & \mathcal{B}(t)\\ \mathcal{B}(t) & \mathcal{A}^*(t)\end{bmatrix}\begin{bmatrix}\hat{a}(0)\\ \hat{b}(0)\end{bmatrix}, \quad (29)$$

where

$$\mathcal{A}(t) = \cos\nu t + \frac{i(l+\delta)}{2\nu}\sin\nu t, \quad (30)$$

$$\mathcal{B}(t) = \frac{ig}{\nu}\sin\nu t, \quad (31)$$

and the effective Rabi frequency ν is defined as

$$\nu = \frac{\sqrt{(2g)^2 + (l+\delta)^2}}{2}. \quad (32)$$

We consider an initial state where all atoms are condensed in the hyperfine state $|a\rangle$ with zero OAM. If we take a number conserving initial state with definite atom number,

$|\Psi(0)\rangle_N=|N,0\rangle_F=|N/2,-N/2\rangle$, then the half population difference $\hat{J}_z=(\hat{b}^\dagger\hat{b}-\hat{a}^\dagger\hat{a})/2$ evolves in time as

$$_N\langle\Psi(0)|\hat{J}_z|\Psi(0)\rangle_N=-N\frac{(l+\delta)^2+(2g)^2\cos(2\nu t)}{2(2\nu)^2}. \quad (33)$$

The total-angular-momentum operator is just proportional to the number operator of the state $|b\rangle$,

$$\hat{L}=l\hat{b}^\dagger\hat{b}=l(\hat{J}+\hat{J}_z), \quad (34)$$

and the fluctuations in angular momentum coincide with the number fluctuations of the state $|b\rangle$. The time evolution of the angular momentum for an initial Fock state is given by

$$_N\langle\Psi(0)|\hat{L}|\Psi(0)\rangle_N=\frac{Nl\sin^2(\nu t)}{1+(l+\delta)^2/(2g)^2}. \quad (35)$$

We note that the maximum population transfer occurs at the resonant two-photon detuning $\delta=-l$, and the parameter g in Eq. (16) describing the single-particle Raman coupling between the LG field and the BECs decreases with increasing winding number l.

We now repeat the same calculation, but using a Glauber coherent state as an example of an initial BEC displaying BBS

$$|\Psi(0)\rangle_\alpha=|\alpha,0\rangle=\sum_{N=0}^{\infty}C_{\alpha,N}|N,0\rangle_F, \quad (36)$$

where

$$C_{\alpha,N}=e^{-|\alpha|^2/2}\frac{\alpha^N}{\sqrt{N!}}, \quad (37)$$

with $|\alpha|^2\equiv\bar{N}$ being the average number of atoms. The number and phase fluctuations of the coherent state are given by $\Delta n=|\alpha|$, and $\Delta\phi\simeq 1/(2|\alpha|)$, respectively. The time evolutions of the half population difference $_\alpha\langle\Psi(0)|\hat{J}_z|\Psi(0)\rangle_\alpha$ and the total angular momentum $_\alpha\langle\Psi(0)|\hat{L}|\Psi(0)\rangle_\alpha$ are easily shown to coincide with Eqs. (33) and (35) with the replacement $N\to\bar{N}$. In other words, in the absence of the atomic collisions, the physical quantities are therefore independent of whether the state of the initial BEC exhibits BBS or not.

B. Collapse and revivals

The two-mode Hamiltonian exhibits a rich variety of quantum dynamics depending on the relative magnitude of the atomic collisions and atom-field coupling, and the OAM of the LG beam. The system dynamics can be categorized into three typical parameter regimes [29], namely (i) the Rabi regime $g\gg\chi N$, (ii) the Josephson regime $g\ll\chi N\ll gN^2$, and (iii) the Fock regime $gN\ll\chi$. Oscillations between the two BEC states are almost perfect in the Rabi regime at the resonance condition $h_z=0$, but the transfer between the coupled BECs reduces as the Josephson regime is approached. In the Fock regime, the Rabi oscillations are suppressed and the number in each internal state is almost a constant, like the case of self-trapping in a double-well potential or the Mott state in optical lattices. The critical point of the self-trapping transition is $\chi N\simeq 4g$, which lies in the Josephson regime (ii). Here we concentrate on the situation where the system is in the Rabi regime, considering for concreteness the parameter values $N=\bar{N}=100$, $\chi=5\times10^{-3}$, and $g=10$, corresponding to a condensate with a mesoscopic total number of atoms. In the following numerical study we choose $l=2$ as a representative example, and take the two-photon detuning as $\delta=-l+(N-1)\chi_-$, so that $h_z=0$. With these parameters we anticipate almost complete Rabi oscillations of the population difference between the two condensate components.

To proceed we introduce two initial states that represent NC and BBS states for the initial BEC. First, for the NC state we choose a state with a well-defined atom number $|N,0\rangle_F$ in Fock-space representation. The subsequent quantum dynamics of the coupled BECs may then be represented in the angular-momentum basis as

$$|\Psi(t)\rangle_N=\sum_{m=-j}^{j}A_m(t)|j,m\rangle, \quad (38)$$

where $j=N/2$, and the normalization is given by $\Sigma_m|A_m(t)|^2=1$. On the other hand, for an initial condition with BBS where the initial state is a coherent state $|\alpha,0\rangle$, the time evolution of the coupled BECs may be represented in the angular-momentum basis as

$$|\Psi(t)\rangle_\alpha=\sum_{N=0}^{\infty}C_{\alpha,N}\sum_{m=-j'}^{j'}A_m^{(j')}(t)\delta_{N,2j'}|j',m\rangle, \quad (39)$$

where there is no dynamical coupling between subspaces with different total number of atoms since the Hamiltonian conserves the atom number [30].

Figure 2 shows the numerically calculated time evolution of $\langle\hat{J}_x\rangle_N$ and $\langle\hat{J}_z\rangle_N$ for an initial Fock state, and of $\langle\hat{J}_x\rangle_\alpha$ and $\langle\hat{J}_z\rangle_\alpha$ for an initial coherent state. In both cases atomic collisions cause the anticipated complete Rabi oscillations between the two BECs to be modulated by a sequence of collapses and revivals, the revivals being a characteristic consequence of the granular nature of the matter wave fields. The components $\hat{J}_{x,y}$ characterize the coherence between the states $|a\rangle$ and $|b\rangle$, while $\hat{J}_z$ corresponds to half their population difference. We note that $\langle\hat{J}_x\rangle$ exhibits a revival in the middle of the collapse of $\langle\hat{J}_z\rangle$ for both coherent and Fock initial states.

There is a significant difference between the period of revivals for the NC and BBS initial states. In the Rabi regime, and for the resonant case $h_z=0$, the collapse time and revival time in the population difference $\langle\hat{J}_z\rangle$ are numerically found to be

$$T_{\text{collapse}}^{(N)}=\frac{\mathcal{C}}{\chi\sqrt{N}},\quad T_{\text{revival}}^{(N)}=\frac{2\pi}{\chi} \quad (40)$$

for the initial Fock state, and

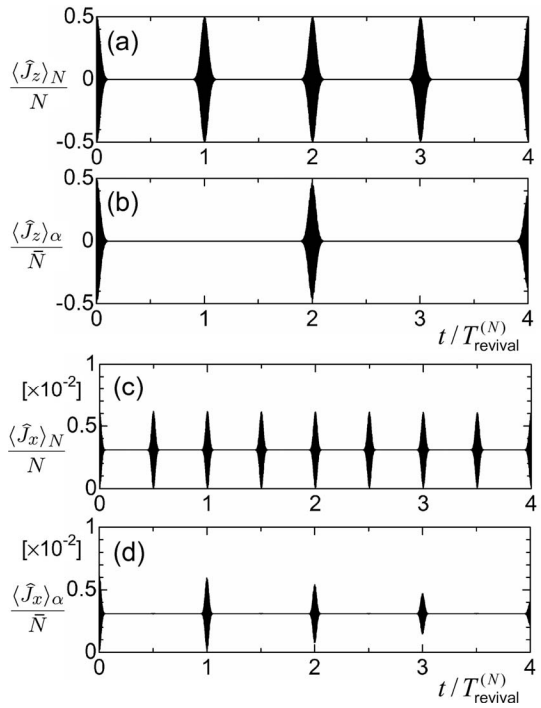

FIG. 2. Time evolutions of (a) $\langle \hat{J}_z \rangle_N$, (b) $\langle \hat{J}_z \rangle_\alpha$, (c) $\langle \hat{J}_x \rangle_N$, (d) $\langle \hat{J}_x \rangle_\alpha$ for $N=\bar{N}=100$, $\chi=5\times10^{-3}$, and $g=10$.

$$T^{(\alpha)}_{\text{collapse}} \simeq T^{(N)}_{\text{collapse}}, \quad T^{(\alpha)}_{\text{revival}} = 2T^{(N)}_{\text{revival}} \tag{41}$$

for the initial coherent state, respectively, where the constant is $\mathcal{C}\simeq 10$. This factor of 2 difference in the revival period is also found in the double-well system and for the Ramsey fringe experiment proposed by Search, and the revival period agrees with that he found for the resonant case [13].

For the sake of completeness we comment briefly on the effect on our findings of selecting a nonzero value of the parameter h_z. For the case $h_z \neq 0$, which would be possible using a Feshbach resonance, the system enters the Josephson regime as χ_- increases, and this reduces the collapse time for both the Fock and coherent states. The Rabi oscillations are then no longer perfect, and the coherent state collapses much faster than the Fock state. Although the revival time becomes longer, the factor of two difference between Fock and coherent initial states remains. This is different from the situation in the Ramsey technique, where the system evolves freely in time (without coupling between the BECs) between the Ramsey pulses and the coupling term proportional to $\hat{J}_x$ in the Hamiltonian is zero. In the present case, by contrast, the Raman coupling is on at all times.

Finally we emphasize that the factor of two difference in revival period depends only on whether the initial state is NC or not. For instance, if the initial state is chosen as number-conserving coherent state with binomial statistics [31], then the period of the revival will still be half that of the Glauber coherent state.

C. Quantized vortex motion

The results of the previous section show that the collapse and revivals in the dynamics of the quantum vortex coupler can be used to test whether the initial state of the BEC is described as a NC state or a BBS state, and these results are in perfect accord with previous works on this topic. However, measuring the components of the angular momentum in Schwinger's representation raises issues of how to detect these quantities. Here we propose to detect the collapses and revivals by monitoring the spatial density profile of the Raman-coupled BECs, and in particular, the motion of the quantized vortices that appear in the profile. Collapse and revival dynamics have previously been observed by monitoring the spatial density profile in a two-component ^{87}Rb BEC [22], and a Raman vortex coupler using LG beams has now been realized experimentally [23]. These experiments were performed for large atom numbers where the granular nature of the matter wave fields is not relevant, but they show that the proposed approach has some validity.

To proceed we investigate how the quantum dynamics can manifest itself in the spatial density profile of the coupled BECs. From Eq. (10), the density operator $\hat{\rho}(\boldsymbol{r},t)$ may be written as

$$\hat{\rho}(\boldsymbol{r},t) = \hat{\Psi}^\dagger(\boldsymbol{r},t)\hat{\Psi}(\boldsymbol{r},t) = \hat{\rho}_0(\boldsymbol{r},t) + \hat{\rho}_1(\boldsymbol{r},t), \tag{42}$$

where

$$\hat{\rho}_0(\boldsymbol{r},t) = |\psi_0(\boldsymbol{r})|^2 \left[\left(1 + \frac{r^{2l}}{l!}\right)\hat{J}(t) - \left(1 - \frac{r^{2l}}{l!}\right)\hat{J}_z(t) \right], \tag{43}$$

$$\begin{aligned}\hat{\rho}_1(\boldsymbol{r},t) &= \frac{r^l|\psi_0(\boldsymbol{r})|^2}{\sqrt{l!}}[\hat{J}_-(t)e^{il\varphi} + \hat{J}_+(t)e^{-il\varphi}] \\ &= \frac{r^l|\psi_0(\boldsymbol{r})|^2}{\sqrt{l!}}[\hat{J}_x(t)\cos(l\varphi) + \hat{J}_y(t)\sin(l\varphi)],\end{aligned} \tag{44}$$

and the total density profile for both atomic states is given by $\langle\hat{\rho}(\boldsymbol{r},t)\rangle = \langle\hat{\rho}_0(\boldsymbol{r},t)\rangle + \langle\hat{\rho}_1(\boldsymbol{r},t)\rangle$.

From this equation we see that the spatial density profile is directly related to the pseudospin components, hence it will also display the collapse and revival phenomenon. Since the qualitative properties of the density profile are the same for both the Fock and coherent initial states, with the caveat that the revival period is twice as long for the coherent state, here we show results for the case of an initial number state.

Figure 3(a) shows the evolution of the density profile $\langle\hat{\rho}(\boldsymbol{r},t)\rangle_N$ over one Rabi oscillation for times sufficiently short that the first collapse is barely noticeable, and Fig. 3(b) shows the corresponding evolution of $\langle\hat{J}_i\rangle_N/N$, $i=x,y,z$ for the number state here times are scaled to the revival time $T^{(N)}_{\text{revival}}$. For the earliest time $t/T^{(N)}_{\text{revival}}=5\times10^{-4}$ in these plots, $\langle\hat{J}_z\rangle_N/N \simeq -1/2$, meaning that the condensate is almost entirely in the nonrotating Gaussian mode, and the left-most gray-scale density profile in Fig. 3(a) shows this Gaussian density profile. As time progresses, however, the Raman coupling transfers more population to the rotating BEC mode with $l=2$, and the second through fourth density profiles in Fig. 3(a) show this process in which two vortex cores with winding number $l=1$ progressively make their way towards the center of the condensate. Halfway through the Rabi oscillation the BEC is composed purely of the rotating state,

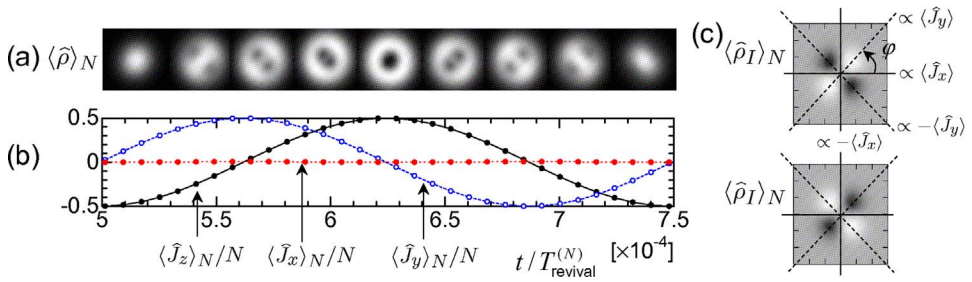

FIG. 3. (Color online) (a) Time sequence of density profiles $\langle\rho(\boldsymbol{r},t)\rangle_N$ given by Eq. (42), and (b) expectation values of the pseudospin components during one Rabi cycle. Solid curve with the filled dots shows $\langle\hat{J}_z\rangle_N$, dotted curve with the open dots $\langle\hat{J}_y\rangle_N$, and dotted curve with the filled dots $\langle\hat{J}_x\rangle_N$, respectively. (c) Off-diagonal part of the density $\langle\rho_I(\boldsymbol{r},t)\rangle_N$ given by Eq. (44). Upper and lower panels show the typical patterns for the first half and latter half of a Rabi cycle, respectively. The alignment of the two density maxima (mimina) rotates by $\pi/2$ anytime when the $\langle\hat{J}_y\rangle_N$ crosses the zero.

corresponding to the time $t/T^{(N)}_{\text{revival}}=6.25\times10^{-4}$ in Fig. 3(b) where $\langle\hat{J}_z\rangle_N/N\simeq1/2$, and the density profile is now that for a pure matter-wave vortex with $l=2$ centered at the origin. For longer times the process reverses up until $t/T^{(N)}_{\text{revival}}=7.5\times10^{-4}$ when the next Rabi oscillation starts.

During a single Rabi oscillation the distance between the two $l=1$ matter-wave vortices is related to the population difference $\langle\hat{J}_z\rangle_N$. The angle of the line joining the two $l=1$ vortex cores (where the density goes to zero) may be understood by looking at the off-diagonal part of the density profile $\langle\rho_I(\boldsymbol{r},t)\rangle_N$. As seen from Eq. (44), the angle of the line joining the vortex cores is determined by the pseudospin components $\langle\hat{J}_x\rangle$ and $\langle\hat{J}_y\rangle$. For example, the spatial distribution of the off-diagonal part of the density profile at the angle $\varphi=0$ is always proportional to $\langle\hat{J}_x\rangle$, whereas at the angle $\varphi=\pi/4$ it is proportional to $\langle\hat{J}_y\rangle$. For the parameters of this example we have that $|\langle\hat{J}_x\rangle_N|\ll|\langle\hat{J}_y\rangle_N|$, see Fig. 3(b). Then, viewing the expectation values of the pseudospin components as parameters on a Bloch sphere, one Rabi oscillation corresponds to a round trip between the south pole ($\langle\hat{J}_z\rangle_N/N=-1/2$) and the north pole ($\langle\hat{J}_z\rangle_N/N=1/2$), with the shortest path being taken on the Bloch sphere. Since the component $\langle\hat{J}_x\rangle$ is small compared to the other two components, the off-diagonal term is approximately given by $\langle\rho_I\rangle\simeq r^l|\psi_0(\boldsymbol{r})|^2\langle\hat{J}_y(t)\rangle\sin(l\varphi)/\sqrt{l!}$, which illustrates the change in profile in Fig. 3(c) for times before and after the system evolves halfway through the Rabi oscillation in Fig. 3(b). When the value $\langle\hat{J}_y\rangle_N$ crosses zero halfway through the Rabi oscillation at $t/T^{(N)}_{\text{revival}}=6.25\times10^{-4}$ in Fig. 3(b), the positions of the off-diagonal density maxima and minima are interchanged. This gives rise to the change in the angle of the line joining the two $l=1$ vortex cores in Fig. 3(a). We remark that if the dynamics takes the longer path on the Bloch sphere, i.e., as happens when $\hat{J}_x$ and $\hat{J}_y$ become comparable and exchange their values, the position of the vortices can rotate around the condensate. Hence the radius and angle of the vortex position generally follow a trajectory on the Bloch sphere.

Figure 4 shows a time sequence of density plots over time scales long enough to allow for a collapse and revival, the lower plot showing the evolution of $\langle\hat{J}_z\rangle_N/N$ versus time. For short times the system undergoes Rabi oscillations as in Fig. 3, but modulated by a collapse envelope are shown for times $t/T^{(N)}_{\text{revival}}<0.1$, in the upper left panel. In the collapse region $0.1<t/T^{(N)}_{\text{revival}}<0.9$ when $\langle\hat{J}_z\rangle_N/N\to0$, the density profile is to all intents and purposes stationary and the vortex cores assume fixed positions, see the central upper panel. Finally, for $t/T^{(N)}_{\text{revival}}>0.9$ the first revival starts, the vortex cores get back into motion, and the Rabi oscillations start again, see the right most upper panel. Thus the motion of the vortex cores in the density profile provides a convenient means to monitor collapse and revivals in the quantum dynamics of the matter wave vortex coupler. Density measurements thus represent a powerful tool to measure the dynamics of the collapse and revivals as well as the motion of the condensate on the Bloch sphere, and as such allow one to measure the factor of two difference in the revival times for initial state displaying Bose broken symmetry or being number conserving.

D. Atom statistics

For completeness we now briefly discuss the atom statistics of the system as it undergoes a series of collapses and revivals. A familiar measure of the atom-number fluctuations is Mandel's Q parameter [32]

$$Q_j=\frac{\langle(\Delta\hat{n}_j)^2\rangle-\langle\hat{n}_j\rangle}{\langle\hat{n}_j\rangle},\quad j=a,b, \tag{45}$$

where $Q=0$ corresponds to a Poissonian, $-1\le Q<0$ to a sub-Poissonian, and $Q>0$ to a super-Poissonian distribution.

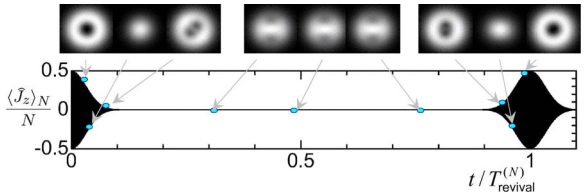

FIG. 4. (Color online) Density profiles $\langle\rho(\boldsymbol{r},t)\rangle_N$ (upper panels) and half population difference $\langle\hat{J}_z\rangle_N/N$ (lower panel) for times allowing for collapse and revivals. The density plots are shown at the times indicated by small circles in the lower panel.

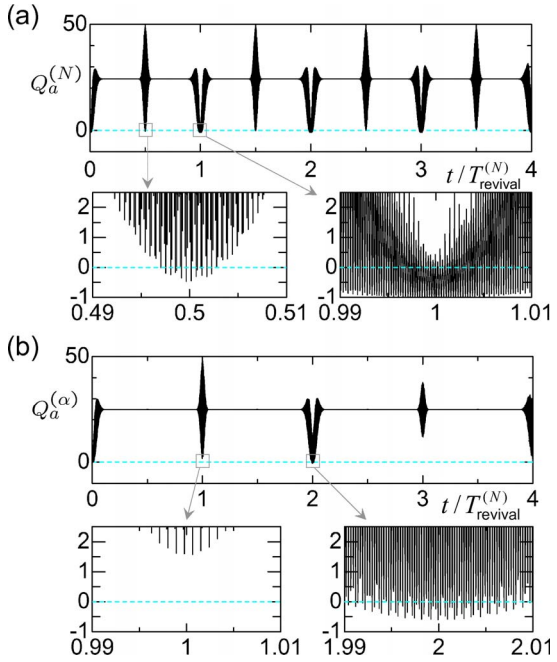

FIG. 5. (Color online) Mandel's Q parameter defined by Eq. (45) for initial (a) Fock and (b) coherent states. The value becomes -1 near the revival for the initial Fock state, while it is always larger than -1.

In particular, $Q=-1$ corresponds to a Fock state with $\langle \Delta n_j \rangle = 0$. As expected and illustrated in Fig. 5, the Mandel parameter also exhibits the factor of two difference in the revival times depending on the U(1) symmetry of the condensate. For the initial Fock state [Fig. 5(a)], $Q_a=-1$ initially, and $Q_a(t)$ returns to that value periodically near the revivals. For an initial coherent state, on the other hand, the Mandel parameter is initially $Q_a=0$. It then becomes negative near the revivals, indicative of a sub-Poissonian distribution, but never reaches the Fock state value $Q_a=-1$. Note also that the average values of Q_a for the coherent and Fock state approach each other as the number of atoms increases.

E. Effects of thermal dissipations

To assess the feasibility of an experimental demonstration of these predictions, we consider the specific example of a ^{87}Rb condensate with Raman coupling between the two hyperfine states $|a\rangle=|F=1,m_F=-1\rangle$ and $|b\rangle=|F=1,m_F=1\rangle$. The trapping potentials of these two states are almost identical, $V_1(\boldsymbol{r}) \simeq V_2(\boldsymbol{r})$. It is experimentally clearly desirable to have a relatively short revival time, so that a tight condensate confinement is preferable. Taking $\omega_r = 2\pi \times 100$ Hz and $\omega_z = 2\pi \times 300$ Hz, the corresponding oscillator lengths are then $d_r \simeq 1$ μm, $d_z \simeq 0.6$ μm. All s-wave scattering lengths are approximately the same, $a_{aa} \simeq a_{bb} \simeq a_{ab} \simeq 5.5$ nm. For this set of parameters, the validity of the two-mode model requires that the total number of atoms has to be $N \lesssim 200$. For the case of an OAM $l=1$, these values result in the dimensionless parameters $G_{aa}=2G_{bb}=2G_{ab} \simeq 3.7 \times 10^{-3}$ and thus $\chi = G_{aa}/2 = 1.8 \times 10^{-3}$ [see Eqs. (15) and (17)]. Typical time scales are then estimated as $T_{\text{Rabi}} \simeq 1.4 \times 10^{-3}$ s, $T_{\text{collapse}}^{(N)} \simeq 0.5$ s, $T_{\text{revival}}^{(N)} \simeq 5.5$ s, and $T_{\text{revival}}^{(\alpha)} \simeq 11.0$ s, respectively. Hence the difference in the revival periods of the Fock and coherent states should be observable in a condensate with a relatively long lifetime on the order of a few tens of second.

We note that there is a caveat with respect to our proposal in that it involves multiply charged matter-wave vortices with winding numbers whose magnitude is greater than one. In particular, it is well known that if a multiply charged vortex is initiated and allowed to evolve freely it will quickly decay into multiple singly charged vortices in the presence of even a small background component of thermal atoms [33]. The decay time τ_d for a doubly quantized vortex ranges from one to a few tens of milliseconds, depending on the total number of atoms.

However, this does not pose a problem for the Raman coupler analyzed here, as the matter-wave vortices are not freely moving, but rather are externally driven by the LG beams. More specifically, the applied LG laser fields continually drive the matter-wave field between the zero-charged ($l=0$) and doubly charged ($l=2$) vortex states with a time period corresponding to the inverse Rabi frequency $T_{\text{Rabi}} \simeq 1.4 \times 10^{-3}$ s. (This is true even in the collapse region where the time-independent density profile arises from an average over many oscillating components with slightly different periods.) Thus, as long as $T_{\text{Rabi}} \ll \tau_d$ there will be negligible decay of the doubly-charged vortex created in any Rabi cycle before it is returned to the zero-charged state and the next Rabi cycle starts.

IV. SUMMARY

In summary, we have studied the quantum dynamics of the vortex coupler using the Laguerre-Gaussian beams. As a consequence of the quantization of the matter-wave field, the atoms are found to undergo a series of collapses and revivals whose period is directly observable as an off-axis motion of the quantized vortex cores that appear in the condensate density. The angle of the vortex also provides direct information on its path on the Bloch sphere that describes its dynamics in the Schwinger representation. An important feature is that the characteristic time scale of the collapse and revivals dif-

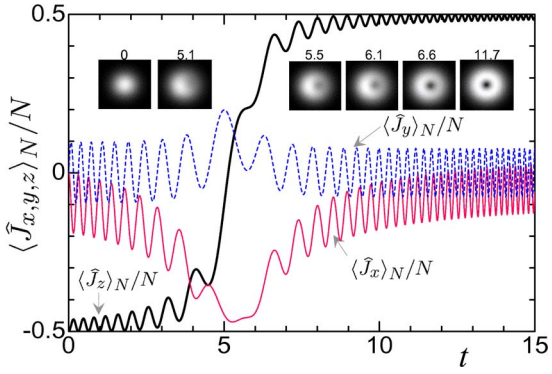

FIG. 6. (Color online) Population transfer from the state $|a\rangle$ to $|b\rangle$ with the linear sweep of the two-photon detuning. The insets and the numbers express the intensity of the interference pattern and the corresponding (dimensionless) time.

fers by the factor 2 depending on whether the description of the condensate is in terms of a number-conserving state or a state with broken U(1) symmetry [10,11,13].

We finally note that instead of generating the collapse and revivals used to test the appropriate theoretical description of the condensate, our scheme can also be modified slightly to permanently transfer the condensate population to the state $|b\rangle$. All that is required is to sweep the two-photon detuning linearly in time at an appropriate rate. We illustrate this technique with the parameters $N=100$, $\chi=5\times10^{-3}$, $g=2$, and $\delta=20-4t$ in Fig. 6. Since both the initial and final states are in the Josephson regime, no detectable collapse and revival occurs in any observables. The $\hat{J}_x$ and $\hat{J}_y$ components have maximum values when the detuning δ crosses the resonance, and a significant change in $\hat{J}_z$ occurs at this point. Note that a population transfer is achievable independently of the U(1) symmetry, although the variances and atom statistics differ significantly in both cases.

ACKNOWLEDGMENTS

We are thankful to Dr. D. Meiser and Dr. B. P. Anderson for fruitful discussions and comments. This work is supported in part by the U.S. Office of Naval Research, by the National Science Foundation, by the U.S. Army Research Office, and by the National Aeronautics and Space Administration.

[1] C. S. Adams and E. Riis, Prog. Quantum Electron. **21**, 1 (1997).
[2] A. Ashkin, J. M. Dziedzic, J. E. Bjorkholm, and S. Chu, Opt. Lett. **11**, 288 (1986).
[3] T. Bourdel, T. Donner, S. Ritter, A. Öttl, M. Köhl, and T. Esslinger, Phys. Rev. A **73**, 043602 (2006).
[4] C. N. Yang, Rev. Mod. Phys. **34**, 694 (1962).
[5] P. W. Anderson, *Basic Notions of Condensed Matter Physics* (Addison-Wesley, Reading, MA, 1984), pp. 229–261.
[6] A. Griffin, *Excitations in a Bose-Condensed Liquid* (Cambridge University Press, Cambridge, UK, 1993), Chap. 3.
[7] A. J. Leggett and F. Sols, Found. Phys. **21**, 353 (1991).
[8] J. Javanainen and S. M. Yoo, Phys. Rev. Lett. **76**, 161 (1996).
[9] Y. Castin and J. Dalibard, Phys. Rev. A **55**, 4330 (1997).
[10] D. F. Walls, M. J. Collett, T. Wong, S. M. Tan, and E. M. Wright, Philos. Trans. R. Soc. London, Ser. A **355**, 2393 (1997).
[11] E. M. Wright, T. Wong, M. J. Collett, S. M. Tan, and D. F. Walls, Phys. Rev. A **56**, 591 (1997).
[12] G. J. Milburn, J. Corney, E. M. Wright, and D. F. Walls, Phys. Rev. A **55**, 4318 (1997).
[13] C. P. Search, Phys. Rev. A **64**, 013612 (2001).
[14] J. Sebby-Strabley, B. L. Brown, M. Anderlini, P. J. Lee, W. D. Phillips, J. V. Porto, and P. R. Johnson, Phys. Rev. Lett. **98**, 200405 (2007).
[15] G. Rempe, H. Walther, and N. Klein, Phys. Rev. Lett. **58**, 353 (1987).
[16] J. A. Yeazell, M. Mallalieu, and C. R. Stroud, Jr., Phys. Rev. Lett. **64**, 2007 (1990).
[17] M. Greiner, O. Mandel, T. W. Hänsch, and I. Bloch, Nature (London) **419**, 51 (2002).
[18] K. P. Marzlin, W. Zhang, and E. M. Wright, Phys. Rev. Lett. **79**, 4728 (1997).
[19] R. Dum, J. I. Cirac, M. Lewenstein, and P. Zoller, Phys. Rev. Lett. **80**, 2972 (1998).
[20] K. T. Kapale and J. P. Dowling, Phys. Rev. Lett. **95**, 173601 (2005).
[21] M. R. Matthews, B. P. Anderson, P. C. Haljan, D. S. Hall, C. E. Wieman, and E. A. Cornell, Phys. Rev. Lett. **83**, 2498 (1999).
[22] M. R. Matthews, B. P. Anderson, P. C. Haljan, D. S. Hall, M. J. Holland, J. E. Williams, C. E. Wieman, and E. A. Cornell, Phys. Rev. Lett. **83**, 3358 (1999).
[23] M. F. Andersen, C. Ryu, P. Cladé, V. Natarajan, A. Vaziri, K. Helmerson, and W. D. Phillips, Phys. Rev. Lett. **97**, 170406 (2006).
[24] A. B. Bhattacherjee, J. Opt. B: Quantum Semiclassical Opt. **4**, 251 (2002).
[25] For an overview of OAM in optics see, for example, *Optical Angular Momentum*, edited by L. Allen, S. M. Barnett, and M. J. Padgett (IOP Publishing, Bristol, 2003).
[26] S. J. van Enk, Quantum Opt. **6**, 445 (1994).
[27] M. J. Steel and M. J. Collett, Phys. Rev. A **57**, 2920 (1998).
[28] Strictly speaking, the frequencies of the harmonic potentials and thus the oscillator lengths for the atomic states $|a\rangle$ and $|b\rangle$ are different. However, this difference can be erased by adjusting (i) the laser frequency so that the $\omega_r^{(a)}=\omega_r^{(b)}$, or (ii) the coupling constant of the interatomic interaction so that $d_r^{(a)}=d_r^{(b)}$.
[29] A. J. Leggett, Rev. Mod. Phys. **73**, 307 (2001).
[30] W. Chen, D. Meiser, and P. Meystre, Phys. Rev. A **75**, 023812 (2007).
[31] F. T. Arecchi, E. Courtens, R. Gilmore, and H. Thomas, Phys. Rev. A **6**, 2211 (1972).
[32] M. O. Scully and M. S. Zubairy, *Quantum Optics* (Cambridge University Press, Cambridge, UK, 1997), pp. 340.
[33] Y. Shin, M. Saba, M. Vengalattore, T. A. Pasquini, C. Sanner, A. E. Leanhardt, M. Prentiss, D. E. Pritchard, and W. Ketterle, Phys. Rev. Lett. **93**, 160406 (2004).